through carefully sized holes in the central air distribution pipe. Because of the decreasing air velocity down the distribution pipe, varying from a maximum at the inlet end down to zero at the opposite end, a significant static pressure gradient is established along the pipe relative to the pressure drop through the matrix. This effect is compensated for by varying the hole size along the length of the pipe. The final design employs 1200 holes in the $3\frac{1}{2}$-in.-diam distribution pipe, located approximately on $\frac{3}{4}$-in. centers, and varying from 0.136-in.-diam at the inlet end to 0.104-in.-diam at the exit end. A static pressure gradient in the outer air flow annulus is avoided by tapering the outside of the matrix so as to maintain a near-constant flow velocity in this passage.

The heating element is a Nichrome V ribbon strung through the bed in three sections, and is designed for direct connection to a three-phase 220-v power line. The heating element is designed to provide a maximum heating time from ambient to 2200°R of 2 hr, without exceeding the element temperature limit of 2600°R. The total power input is 40 kw.

The insulation material used to protect the heat exchanger shell is 1-in.-thick Cerefelt CRF600, a Johns-Manville ceramic fiber felt material that is readily formable when wet, but relatively rigid when dry. It is held in place with a Nichrome wire screen. The equilibrium temperature of the heat exchanger surface is approximately 350°F for an internal temperature of 1800°F, and an ambient temperature of 70°F.

System Performance

Since the facility was completed in June 1967, it has been used for 27 rocket test firings. In addition, approximately 40 "air-only" tests have been performed for checkout and calibration purposes. In all of this testing only two failures have occurred. One of these resulted from some apparently faulty parts in the pressure regulator, the other failure was in the ceramic supports for the Nichrome heating element. The support system was subsequently redesigned, and no further difficulties have been experienced.

The air temperature distribution at the entrance to the test section was measured in a series of tests with 12 uniformly distributed, fast response thermocouples. A slight vertically oriented nonuniformity was noted which is attributed to convection currents in the pebble bed during the heating cycle. An additional nonuniformity, particularly during the first second of operation, is caused by heat transfer to the plenum walls and rocket motor housing. After the first second, the standard deviation of the 12 thermocouples is generally less than 20°F, which is considered satisfactory. For the rocket motor firings, the 12 thermocouple outputs are averaged together electrically, and recorded on a single channel.

Because of the transient nature of the tests and the location of the air flow nozzle upstream of the heat exchanger, a correction is necessary to obtain the air flow rate at the test section. This correction is equal to the rate of accumulation of air within the heat exchanger and plenum, and is determined from the known volumes and the measured rates of change of air temperature and pressure. The magnitude of this correction varies up to 5%. An additional correction, obtained from Ref. 2, for the real gas effects in the flow nozzle is also applied. These corrections have been verified in a series of tests in which the test section was replaced with another critical flow nozzle. With the preceding corrections applied, the two flow rates agree within 1% after the initial starting transient of about 1 sec.

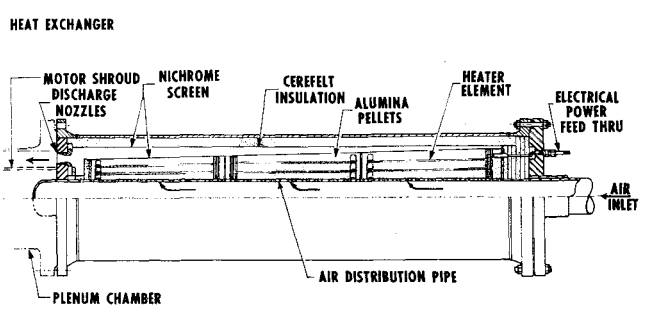

Fig. 2 Heat exchanger assembly.

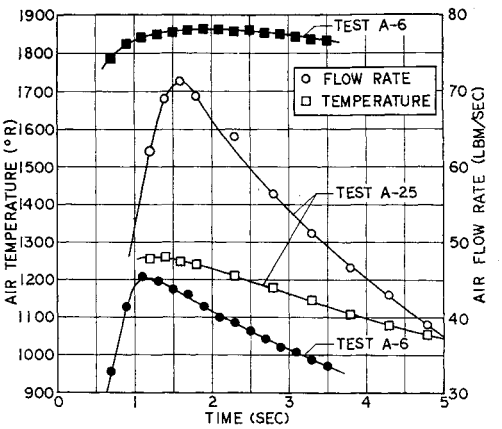

Fig. 3 Typical performance data.

Initial tests disclosed a severe "ringing" of the thrust measuring system, i.e., poorly-damped oscillations in response to impulsive thrust forces. This was improved to an acceptable level by means of felt pads isolating the air storage bottles and heat exchanger from the thrust stand bed. Ringing time was reduced to about $\frac{1}{2}$ sec.

Typical data from two test firings are shown in Fig. 3. Test A-6 illustrates operation at a high air temperature and moderate air flow rate, simulating Mach 3.9 at 20,000 ft altitude. Test A-25 shows operation at a high air flow rate (the facility's limit) and a moderate temperature.

Conclusions

The facility fulfils its design objectives and provides, at a very low cost, a capability for testing small- to medium-scale air-augmented rocket systems up to Mach 4 with clean air and with a highly reliable and accurate thrust measurement. It is believed that this combination of desirable attributes is not obtainable with any other type of system.

References

[1] Brown, G. et al., *Unit Operations*, Wiley, New York, 1950.

[2] Johnson, R. C., "Real Gas Effects in Critical-Flow-Through Nozzles and Tabulated Thermodynamic Properties," TN D-2565, Jan. 1965, NASA.

Thermal Stresses in Hollow Graphite Cylinders with Asymmetric Heating

SAM TANG*

Lockheed Missiles & Space Company, Sunnyvale, Calif.

I. Analysis

THERMAL stresses in anisotropic hollow cylinders due to axisymmetric temperature distribution have been investigated during the last few years for application of rocket

Received October 16, 1967; revision received December 20, 1967.

* Research Scientist Associate, Structures, Research, and Development Division.

Table 1 Numerical examples for graphites

	Grade *ATJ*	Grade *ZTA*
$E_r = E_\theta$, 10^6 psi	1.40	2.76
E_z, 10^6 psi	1.15	0.76
ν_{zr}	0.11	0.2
$\nu_{r\theta}$	0.11	0.2
$\alpha_r = \alpha_\theta$, 10^{-6}/°C	2.3	0.6
α_z, 10^{-6}/°C	3.5	9.0
$\bar{\sigma}_r$[a] $= \bar{\sigma}_\theta$ (tension), psi	3260	4380
$\bar{\sigma}_r = \bar{\sigma}_\theta$ (compression), psi	8330	7100

[a] $\bar{\sigma}_r = \bar{\sigma}_\theta$ = fracture stress.

nozzles or re-entry vehicles.[1-5] However, there are situations where the cylinder will be subjected to one-sided aerodynamic heating, e.g., due to a re-entry maneuver within the atmosphere.[6] The purpose of this Note is to analyze stresses of anisotropic hollow cylinders subjected to asymmetric temperature distribution, which may be induced by a steady-state one-sided aerodynamic heating. The analysis is based on the following simplifying assumptions: 1) infinitesimal elasticity theory neglecting effects of coupling and inertia[7]; 2) stress-strain relations obey generalized Hooke's Law; 3) the materials are transversely-isotropic (for example, graphite materials); 4) the principal axes of anisotropy coincide with the principal axes of the cylinder; 5) temperature distribution can be expressed as Fourier series; 6) the condition of plane strain is used; and 7) material parameters are constant.

With these assumptions, the displacement-stress relations in polar coordinates are given as follows[8,9]:

$$\begin{aligned} \partial u/\partial r &= \beta_{11}\sigma_r + \beta_{12}\sigma_\theta + \alpha_{13}T \\ \partial v/r\partial\theta + u/r &= \beta_{12}\sigma_r + \beta_{22}\sigma_\theta + \alpha_{13}T \\ \partial u/r\partial\theta + \partial v/\partial r - v/r &= \tau_{r\theta}/G_{12} \end{aligned} \tag{1}$$

with

$$\begin{aligned} \beta_{ij} &= a_{ij} - a_{i3}a_{j3}/a_{33} \qquad i,j = 1,2 \\ \alpha_{13} &= \alpha_1 - a_{13}\alpha_3/a_{33} \end{aligned} \tag{2}$$

where u and v are displacement components in r and θ directions, respectively, α_i is thermal expansion coefficient, and σ_i is stress.

The coefficients of a_{ij} in terms of technical constants are given by[8]

$$\begin{aligned} a_{11} &= a_{22} = E_1^{-1} \qquad a_{33} = E_3^{-1} \\ a_{12} &= -\nu_{12}/E_1 = -\nu_{21}/E_1 \\ a_{13} &= -\nu_{31}/E_3 = -\nu_{13}/E_1 \end{aligned} \tag{3}$$

where the indices 1, 2, 3 are referred to r, θ, z directions, respectively, in cylindrical coordinates; E_1 and E_3 are the Young's moduli (for tension-compression) in plane and axial directions; ν_{13} is the Poisson's ratio which characterizes the compression in the direction z for in-plane tension and so forth; G_{12} is the in-plane shear modulus. Introducing the stress function F such that

$$\begin{aligned} \sigma_r &= \partial F/r\partial r + \partial^2 F/r^2\partial\theta^2 \\ \sigma_\theta &= \partial^2 F/\partial r^2 \\ \tau_{r\theta} &= -\partial(\partial F/r\partial\theta)/\partial r \end{aligned} \tag{4}$$

the equations of equilibrium will be automatically satisfied. The displacement components u and v in Eqs. (1) can be eliminated by differentiation and combination, and, due to the in-plane isotropy, relation exists among β_{11}, β_{12}, and G_{12}, that is,[10]

$$\beta_{11} - \beta_{12} = (2G_{12})^{-1} = (1 + \nu_{12})/E_1 \tag{5}$$

The equation of compatability in terms of stress function F can, therefore, be simplified to the following form:

$$\nabla^4 F + K_a \nabla^2 T = 0 \tag{6}$$

with $K_a = \alpha_{13}/\beta_{11}$, where ∇^4 and ∇^2 are the two-dimensional biharmonic and harmonic operators, respectively. Equation (6) has the same form as the compatability condition of isotropic material except that the constant K_a is different. Substitution of Eqs. (2) and (3) yields

$$K_a = [(\alpha_1 + \alpha_3\nu_{31})/(1 - \nu_{13}\nu_{31})]E_1 \tag{7}$$

For isotropic material, if we let $\nu_{13} = \nu_{31} = \nu$, and $E_1 = E$, then Eq. (7) may be simplified to

$$K_i = \alpha E/(1 - \nu) \tag{8}$$

where the subscripts a and i denote anisotropic and isotropic materials, respectively.

The boundary conditions and Michell's conditions[7,10] for multiply connected cross sections are essentially the same as isotropic case with K_i replaced by K_a. The temperature distribution due to steady-state, one-sided heating will satisfy the following known equation:

$$\nabla^4 T = \partial^2 T/r^2\partial\theta^2 + \partial(r\partial T/\partial r)/r\partial r = 0 \tag{9}$$

Observe that the stress formulation of transversely isotropic cylinders here, i.e., Eqs. (6) and (9), are identical with that of isotropic cylinders except the contant K_a given by expression (7) is different from the isotropic material K_i in expression (8). Hence, the solution of isotropic material[7] may be used here with the replacement of K_i with K_a. It is convenient to express both the temperature and the stress function in terms of Fourier's series, and, it has been shown[7] that due to the restriction of Michell's conditions, all the higher harmonics of the plane temperature distribution do not contribute to thermal stresses [and noting that the constant as well as the linear temperature distributions (in $x = r\cos\theta$, or in $y = r\sin\theta$) has no contribution in stresses and can be neglected]. Hence, the plane-harmonic temperature distribution which satisfies Eq. (9) has the following form:

$$T(r,\theta) = T_0 \log(r/a) + A_0 \cos\theta/r + B_0 \sin\theta/r \tag{10}$$

where T_0, A_0 and B_0 are constants.

Finally, the in-plane stresses caused by plane-harmonic temperature distribution for transversely isotropic cylinders with inside radius a and outside radius b, and with traction-free boundary conditions, are given by

$$\begin{aligned} \sigma_r &= K_a\left\{\frac{T_0}{2}\left[\frac{(b/r)^2(r^2 - a^2)\log(b/a)}{(b^2 - a^2)} - \log\left(\frac{r}{a}\right)\right] + \right. \\ &\qquad \left. \frac{r(1 - a^2/r^2)(1 - b^2/r^2)(A_0\cos\theta + B_0\sin\theta)}{2(a^2 + b^2)}\right\} \\ \sigma_\theta &= K_a\left\{\frac{T_0}{2}\left[\frac{(b/r)^2(r^2 - a^2)\log(b/a)}{(b^2 - a^2)} - \log\left(\frac{r}{a}\right) - 1\right] + \right. \\ &\qquad \left. \frac{r(A_0\cos\theta + B_0\sin\theta)[3 - (a^2 + b^2)/r^2 - a^2b^2/r^4]}{2(a^2 + b^2)}\right\} \\ \tau_{r\theta} &= \frac{K_a r(1 - a^2/r^2)(1 - b^2/r^2)(A_0\sin\theta - B_0\cos\theta)}{2(a^2 + b^2)} \end{aligned} \tag{11}$$

The displacement components u and v may be obtained by integration of Eqs. (1), after the substitution of expressions (11) into it.

II. Numerical Examples and Conclusions

Observe that all the in-plane stresses in expressions (11) are proportional to the constants K_a for anisotropic, and K_i for isotropic case. In order to demonstrate the significance of the present analysis, for the same given temperature distribution, the stresses obtained for the transversely isotropic material will be compared to the stresses using in-plane material properties for the isotropic case. This is equivalent to the computing of the K_a/K_i ratio. Numerical examples will be given for two different graphites; their properties are given in Table 1[4]:

From expressions (7) and (8) the K_a/K_i ratio may be written as follows:

$$K_a/K_i = (\alpha_r + \alpha_z\nu_{zr})(1 - \nu_{r\theta})/\alpha_r(1 - \nu_{rz}\nu_{zr}) \qquad (12)$$

The stress ratio K_a/K_i for grade ATJ and grade ZTA graphites are obtained by inserting numerical values from Table 1 into expression (12), that is,

$$\text{grade } ATJ \qquad K_a/K_i = 1.045$$

$$\text{grade } ATJ \qquad K_a/K_i = 3.78$$

It can be seen that the K_a/K_i ratio depends strongly on the two coefficients of the linear thermal expansion α_r and α_z. The anisotropy in thermal expansion for grade ATJ graphite is small; hence the stress ratio K_a/K_i shows no significant deviation from unity. However, the anisotropy in thermal expansion for grade ZTA is very large, and the stress ratio is almost 4.

For re-entry vehicles maneuvering within the atmosphere, due to the uneven aerodynamic heating, the temperature on one side of the cylinder can be heated up to several thousand degrees of Farenheit, whereas the temperature on the other side can be just several hundred degrees Farenheit. And significant thermal stresses will be induced by asymmetric heating. An arbitrary numerical example will be given here. The temperatures on the outside of the cylinder are assumed to be 4500°F on the hot side and 200°F on the cool side; on the inside of the cylinder the corresponding high and low temperatures are assumed to be 200°F and 100°F, respectively. The dimensions of the cylinder are taken as a = 3 in., b = 4 in. The maximum tensile and compressive tangential stresses located on the cool and hot side of the cylinder can be calculated for ZTA graphite by using isotropic analysis:

$$(\sigma_\theta) \text{ max. tens.} = 1700 \text{ psi}$$

$$(\sigma_\theta) \text{ max. comp.} = 1900 \text{ psi}$$

which is below the fracture stresses given in Table 1. However, when anisotropy is taken into account, the maximum tangential stresses become

$$(\sigma_\theta) \text{ max. tens.} = (3.78) \times (1700) = 6400 \text{ psi}$$

$$(\sigma_\theta) \text{ max. comp.} = (3.78) \times (1900) = 7200 \text{ psi}$$

which exceed the given fracture stresses in Table 1 and catastrophe will occur to the cylinder.

It can be concluded that for materials with very large anisotropy in thermal expansion, the stresses obtained in the present analysis could be several times higher than those by using assumption of isotropic materials. Hence, thermal stresses are important design considerations for graphite materials with large anisotropy in thermal expansions.

References

[1] Batchelor, J. D. et al., "Improvement of the Usefulness of Pyrolytic Graphite in Rocket Motor Applications," Quarterly Progress Report, June-Aug. 1961, Atlantic Research Corp., Alexandria, Va.

[2] Garber, A. M., "Pyrolite Materials for Thermal Protection Systems," *Aerospace Engineer*, Vol. 22, No. 1, Jan. 1963, pp. 126–137.

[3] Longo, R., "Thermal Stresses in a Hollow Anisotropic Cylinder," *Eighth Midwestern Mech. Conference at Case Institute of Technology*, Cleveland, Ohio, April 1–3, 1963.

[4] Weng, T.-L., "Thermal Stresses in Anisotropic Hollow Cylinders," *Journal of Basic Engineering*, June 1965, pp. 391–397.

[5] Tang, S., "Thermal Stresses in Cylindrically Anisotropic Temperature-Dependent Multi-Layered Hollow Cylinders," Rept. J-17-67-1, March 1967, Lockheed Missiles & Space Co., Sunnyvale, Calif.

[6] Riedinger, L. A., and Johnson, R. R., "Missiles and Space Structures," *Space/Aeronautics*, July 31, 1967, pp. 54–58.

[7] Boley, B. A. and Wiener, J. H., *Theory of Thermal Stresses*, Wiley, New York, 1960, Chap. 2.

[8] Lekhnitskii, S. G., *Theory of Elasticity of an Anisotropic Elastic Body*, translated by P. Stern, Holden Day, San Francisco, 1963, Chap. 4.

[9] Hearmon, R. F. S., *Applied Anisotropic Elasticity*, Oxford University Press, London, 1961, Chap. 5.

[10] Timoshenko, S. and Goodier, J. N., *Theory of Elasticity*, McGraw-Hill, New York, 1951, Chap. 14.

Linear Attitude Programs Applied to the Guidance of European Space Vehicles, and Comparison with the Optimal Control Law

A. Benoît*

Groupe d'Etudes de Technologie Spatiale, sprl, Brussels, Belgium

Nomenclature

k,m = mass flow rate and mass, respectively
r, v = magnitudes of position and velocity vectors, respectively
T = thrust
x_j, v_j = jth (j = 1,2) components of position and velocity vectors, respectively
v_r = radial velocity
α = control angle, angle between the thrust vector and the the axis ox_1, $\alpha_1 = \alpha$, $\alpha_2 = \pi/2 - \alpha$
θ = polar argument, angle between ox_1 and position vector
μ_0 = gravitation constant
ϕ = control angle, angle between position and thrust vectors
ω = angular velocity
ψ = control angle

Subscripts

i = initial state
f = final conditions at burnout of upper stage

Introduction

In the course of trajectory studies conducted at Groupe d'Etudes de Technologie Spatiale (G.E.T.S.), it appeared that small deviations of the control program from the optimal control derived from Pontryagin's principle had practically no effect on the trajectory and implied minor propellant penalties to achieve the final orbit. With the use of inertial guidance in view, this observation has been elaborated to

Received August 25, 1967; revision received December 26, 1967.

* Associate Director; also Maître de Conférences, Department of Applied Mathematics, Catholic University of Louvain, Heverlee, Belgium. Member AIAA.